

Highlights in astroparticle physics: muons, neutrinos, hadronic interactions, exotic particles, and dark matter — Rapporteur Talk HE2 & HE3

J.R. Hörandel

Department of Astrophysics, IMAPP, Radboud University Nijmegen, 6500 GL Nijmegen, The Netherlands — <http://particle.astro.ru.nl>

Recent results presented at the International Cosmic Ray Conference in Beijing will be reviewed. Topics include HE2: "Muons and Neutrinos" and HE3: "Interactions, Particle Physics Aspects, Cosmology".

keywords: muons, neutrinos, neutrino telescopes, hadronic interactions, exotic particles, dark matter

1 Introduction

The 32nd International Cosmic Ray Conference was held in August 2011 in Beijing. About 150 papers were presented in the sessions HE2: "Muons and Neutrinos" and HE3: "Interactions, Particle Physics Aspects, Cosmology". Some of the highlights presented at the conference will be reviewed.

A wide spectrum of (astro-)physical questions is addressed in the papers covered by this rapporteur. The common theme seems to be "upper limits and bounds". The topics include

- Underground experiments, measuring the muon flux from air showers, find evidence for anisotropies in the arrival direction of cosmic rays with TeV energies (Sect. 2).
- The sensitivity of neutrino oscillation searches with water/ice Čerenkov detectors has been reported. Supernova searches indicate that the rate of gravitational stellar collapses in the Galaxy is less than 0.13 events/year (Sect. 3).
- The big neutrino telescopes ANTARES and IceCube are fully operational. Limits on the diffuse neutrino flux reach sensitivities around $10^{-8} \text{ GeV cm}^{-2} \text{ s}^{-1} \text{ sr}^{-1}$. No point sources have (yet) been found (Sect. 4).
- A new method has been introduced, the "end-point formalism", to calculate electromagnetic

radiation from any kind of particle acceleration (Sect. 5).

- Muons are used in a geophysical application for tomography of a volcano (Sect. 6).
- New projects are underway to detect high-energy neutrinos: KM3NeT in the Mediterranean Sea, as well as ARA and ARIANNA on the Antarctic continent (Sect. 7).
- First data from the Large Hadron Collider (LHC), in particular from the forward detector LHCf, yield new insight into hadronic interactions, which are of great importance to describe the development of extensive air showers (Sect. 8).
- New upper limits on magnetic monopoles reach sensitivities of the order of $10^{-18} \text{ cm}^{-2} \text{ s}^{-1} \text{ sr}^{-1}$. Searches for antinuclei indicate that there is less than 1 antihelium nucleus per 10^7 helium nuclei in the Universe (Sect. 9).
- Astrophysical dark matter searches yield upper limits for the velocity-weighted annihilation cross section of the order of $\langle\sigma v\rangle < 10^{-24} \text{ cm}^3 \text{ s}^{-1}$ (Sect. 10).

2 HE 2.1 Muon experiments

2.1 Cosmic-ray anisotropy

The muons registered with GeV energies in underground muon detectors are produced in air showers with TeV energies. Thus, studying the arrival directions of muons in underground facilities provides a mean to study the arrival directions of TeV primary cosmic rays.

At present, the biggest underground muon detector is IceCube at the South Pole. It is comprised of a 1 km^3 water/ice Čerenkov detector at a depth below 1450 m w.e. [1] {BENZVI #306}.¹ The detector is composed of 80 strings, each equipped with 60 optical sensor modules. A surface array (IceTop) consists of 81 stations, each composed of 2 Čerenkov detector water ice tanks, read out by two optical sensors, respectively.

With the more than $32 \cdot 10^9$ events recorded, it is possible to probe the southern sky for per-mille

¹References in {} refer to the Proceedings of the 32nd International Cosmic Ray Conference, Beijing (2011) and to the slides available on the conference web site <http://icrc2011.ihep.ac.cn/> {(first) author name #paper number}.

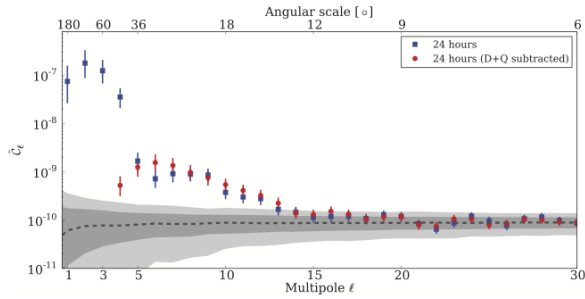


Figure 1: Angular power spectra for the cosmic ray intensity observed by IceCube, see also Fig. 2 [1] {BENZVI #306}.

anisotropy on all angular scales in the arrival direction distribution of cosmic rays. A power spectrum analysis of the relative intensity map of the cosmic-ray flux reveals that the arrival direction distribution is not isotropic, see Fig. 1. Significant structures are seen on several angular scales: a large-scale structure in the form of a strong dipole and a quadrupole, as well as small-scale structure on scales between 15° and 30° . The skymap exhibits several localized regions of significant excess and deficit in cosmic-ray intensity, see Fig. 2. The IceCube observations complement measurements from other detectors in the northern hemisphere, such as the Milagro experiment. The origin of this anisotropy is still unknown.

Another detector in the northern hemisphere is the MINOS neutrino oscillation experiment {DE JONG #1185}. It is comprised of a near and a far detector, two steel-scintillator sampling calorimeters, installed at 100 m and 700 m underground, respectively. Muon data from the near detector have been used to investigate the arrival direction of cosmic rays. A sky map of the significances indicates anisotropies which are compatible with observations by ARGO-YBJ. A projection of the arrival directions on the right ascension axis yields a relative anisotropy amplitude on the order of 0.1%.

2.2 Annual modulation

Annual variations in the (average) temperature profile of the atmosphere alter the air density and, thus, influence the development of air showers. This affects in particular the decay of pions into muons and yields to a seasonal modulation of the observed muon flux.

The BOREXINO solar neutrino detector is located at Gran Sasso National Laboratory below a rock coverage corresponding to about 3800 m w.e. {D'ANGELO #510}. It is a liquid scintillation de-

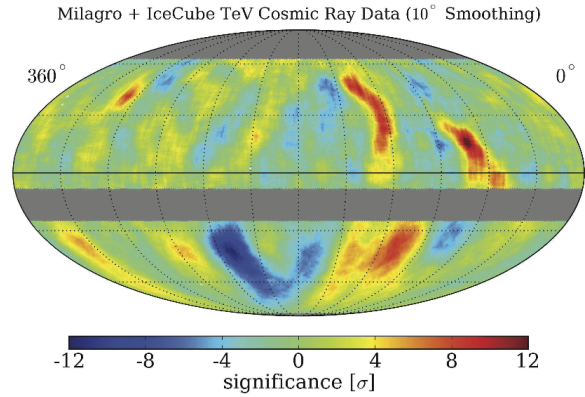


Figure 2: Arrival directions of TeV cosmic rays observed by IceCube and Milagro [1] {BENZVI #306}.

tector with an active mass of about 1.33 kt. The measured muon flux as function of time (see Fig. 3) exhibits a seasonal modulation with an amplitude of 1.5%. The muon flux reaches its maximum at day 186.2 ± 0.4 .

It is remarkable that the measured muon phase almost agrees with the phase of a dark matter signal, claimed by the DAMA experiment at the same location [2]. The maximum of the dark matter signal is observed on June 2nd (day 152). This correlation has also been pointed out in a recent paper [3], using muon flux measurements from the LVD detector. It remains unclear if the seasonal modulation of the underground muon flux significantly influences the observed dark matter signal, after taking into account various measures to reduce the muon-related background.

2.3 Solar modulation

Solar modulation of Galactic cosmic rays is investigated with GRAND {POIRIER #1292}. This is an array of 64 proportional wire chamber stations dispersed in an area of $100 \text{ m} \times 100 \text{ m}$. It continuously monitors the muon flux recorded for about 20 years. The muon data extend the energy range covered by the world-wide neutron monitor network to higher energies. An example is the Forbush decrease on October 29th, 2003, when GRAND registered a sudden intensity drop of 8%. In addition, the direction of the incoming muons is recorded, giving hints of the disturbances in the structure of the heliosphere during a Forbush decrease.

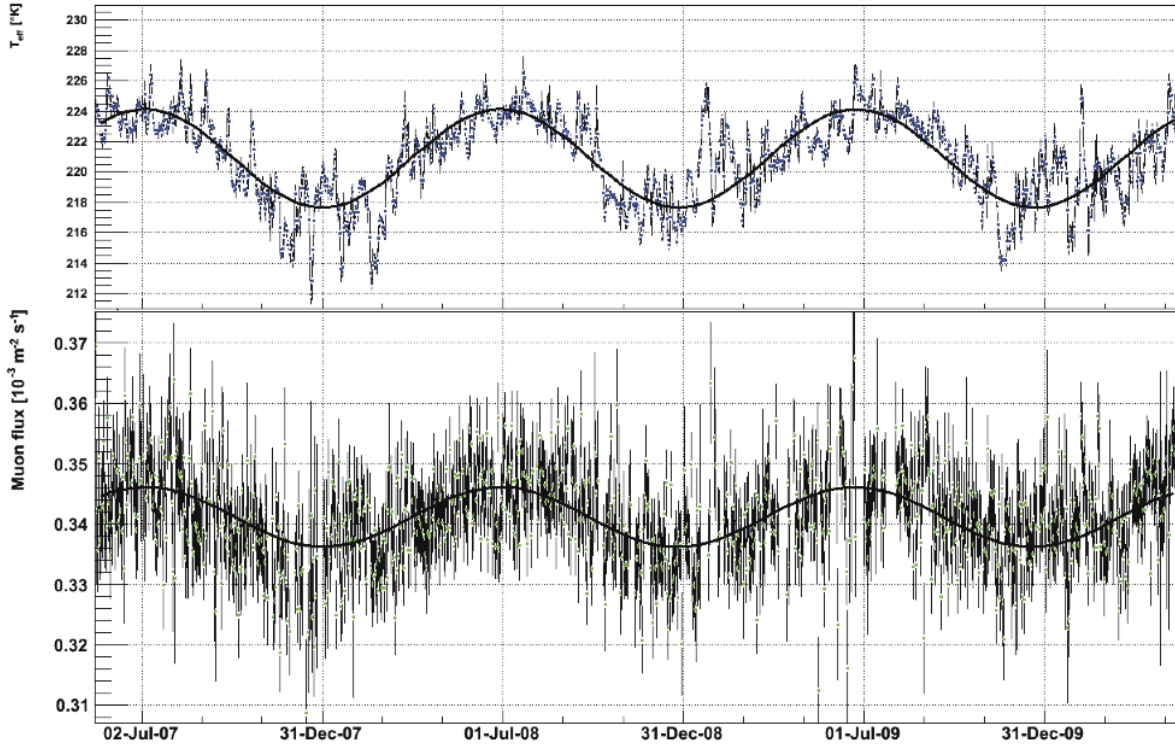


Figure 3: Cosmic-ray induced muon flux observed by BOREXINO as function of time {D'ANGELO #510}.

2.4 Muon interactions

When a high-energy muon traverses matter, such as Antarctic ice, catastrophic energy losses occasionally occur {BERGHAUS #85}. With IceCube the longitudinal profile of such events is reconstructed. This provides a calorimetric measurement of the cascades with TeV energies. The technique is used to extend the measured atmospheric muon spectrum to higher energies up to 500 TeV.

A similar method is applied in the ANTARES neutrino telescope to reconstruct the energy of electromagnetic showers induced by muons in water {MANGANO #158}. The cascades are induced by TeV muons via pair production and bremsstrahlung. Muons with energies up to 100 TeV have been reconstructed.

In extensive air showers muons with high transverse momentum p_T are occasionally produced {GERHARDT #323}. The dominant production processes are the semileptonic decay of heavy quarks and the decay of high p_T kaons and pions in jets. High p_T muons manifest themselves in the data as single muons separated a few hundred meters from the shower core. IceCube with its surface detector IceTop is well suited to study such effects. High p_T muons can be reconstructed with a mini-

muon resolvable $p_T = 8$ GeV for a 1 TeV muon. A data sample of slightly more than 100 days, taken during the construction phase of the detector has been analyzed. No high p_T muon has been found.

2.5 Muon charge ratio

Recent measurements of the atmospheric muon charge ratio for momenta around 1 GeV/c are in agreement with expectations from calculations {BRANCUS #400} {ABDOLAH #749}.

3 HE 2.2 Solar, atmospheric, and related neutrino experiments

In present experiments, neutrinos are measured over a wide energy range. An overview on several detectors and their energy range is given in Fig. 4. Astrophysical neutrinos are expected from MeV energies (solar neutrinos) up to the EeV range (presumably extragalactic sources). The properties of neutrinos are investigated using neutrinos generated in nuclear reactors (MeV regime) and accelerators (GeV regime). Recent results on neutrino os-

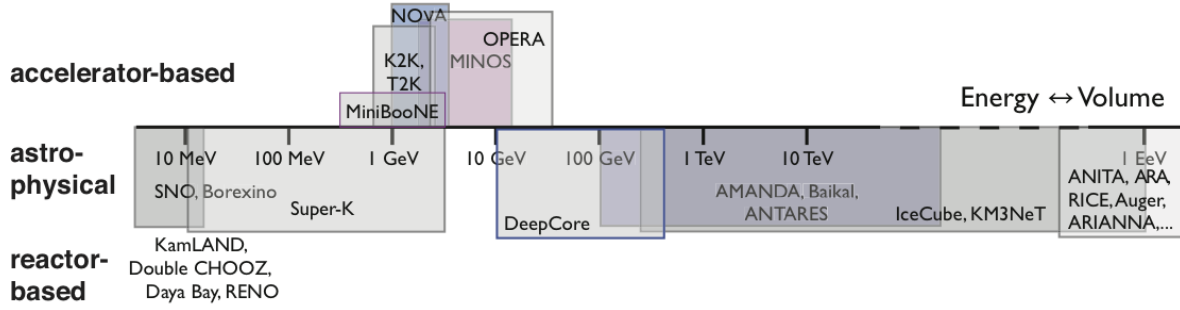


Figure 4: Energy range of various neutrino detectors, after {HA #324}.

cillation measurements are discussed in Sect. 3 and the detection of high-energy neutrinos in Sect. 4.

Neutrino oscillations are commonly described in terms of the L/E dependence, where E is the neutrino energy and L its oscillation path length [4]. For a neutrino telescope such as ANTARES or IceCube, detecting neutrinos crossing the Earth, L can be translated as $2R \sin \Theta$, R being the Earth radius and Θ the angle between the neutrino direction and the vertical axis ($\Theta = \pi/2$ for a vertical upgoing neutrino). Within the two-flavor approximation, the ν_μ survival probability can then be written as

$$P(\nu_\mu \rightarrow \nu_\mu) \approx 1 - \sin^2 2\vartheta_{23} \sin^2 \left(2.54R \frac{\Delta m_{23}^2 \sin \Theta}{E} \right)$$

ϑ_{23} and Δm_{23}^2 being respectively the mixing angle and the squared mass difference of the involved mass eigenstates (with R in km, E in GeV and Δm_{23}^2 in eV^2). According to recent results from the MINOS experiment [5], the first minimum in the muon neutrino survival probability $E/\sin \Theta$ occurs at about 24 GeV. This energy range can be reached with modern neutrino telescopes.

3.1 ANTARES

The ANTARES neutrino telescope is located in the Mediterranean Sea, 40 km south of the French coast at a depth of about 2500 m below sea level. The detector is an array of photomultiplier tubes arranged on 12 vertical detector lines. Each string is comprised of up to 25 floors, each composed of a triplet of optical modules.

The ANTARES collaboration plans to search for neutrino oscillations {GUILLARD #819}. Studies have shown that a clean sample of atmospheric neutrinos with energies as low as 20 GeV can be isolated with the neutrino telescope. The expected sensitivity after 1000 days, corresponding to a total measuring time of four to five years of data-taking, is shown in Fig. 5. The number of expected events

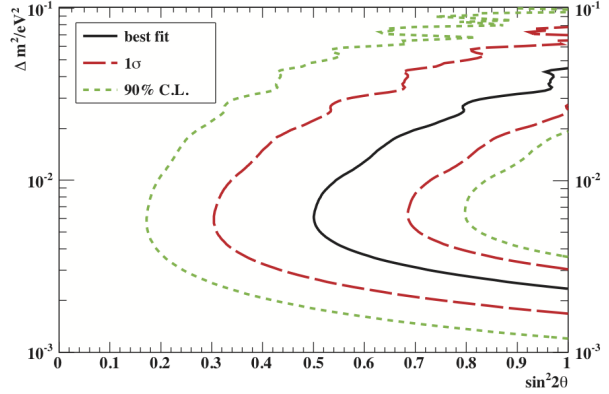


Figure 5: Expected sensitivity of ANTARES to atmospheric neutrino oscillation parameters after 1000 days measuring time {GUILLARD #819}.

is roughly one per day, which for 1000 days leads to a statistical error of about 3% (≈ 30 events). According to these results, although not competitive with dedicated experiments, ANTARES should be sensitive to neutrino oscillation parameters through the disappearance of atmospheric muon neutrinos.

3.2 IceCube

The IceCube detector has an extension to measure neutrinos with lower energies, IceCube DeepCore {HA #324}. This are eight strings in the center of the array which contain additional optical sensors at the bottom of the instrument with a spacing optimized for lower energies.

IceCube DeepCore can study atmospheric neutrino oscillations through a combination of its low energy reach, as low as about 10 GeV, and its unprecedented statistical sample, of about 150000 triggered atmospheric muon neutrinos per year {EULER #329}. As described above, the muon neutrino disappearance minimum and tau neutrino appearance maximum are expected at about 25 GeV, which is considerably lower in energy than typical

IceCube neutrino events, but higher than the energies at which accelerator-based experiments have detected oscillations. ν_μ disappearance and ν_τ appearance from neutrino oscillations can be measured in IceCube. Simulations indicate that for certain oscillation parameters, the measured ν_μ flux is expected to differ by about a factor of two from the flux expected without oscillations.

IceCube is also suited to serve as a supernova detector by monitoring the optical module counting rates across the array {BAUM #1137}. It is expected to detect subtle features in the temporal development of MeV neutrinos from the core collapse of nearby massive stars. For a supernova at the Galactic center, its sensitivity matches that of a background-free megaton-scale supernova search experiment and is expected to trigger on supernovae with about 200, 20, and 6 standard deviations at the Galactic center (10 kpc), the Galactic edge (30 kpc), and the Large Magellanic Cloud (50 kpc), respectively.

3.3 Super-Kamiokande

The Super-Kamiokande detector, one of the experiments establishing neutrino oscillations [6, 7], has recently been upgraded with new electronics {CARMINATI #723} and is now capable of detecting thermal neutrons from neutrino interactions {ZHANG #353}. The objective is to identify low-energy anti-neutrinos via inverse beta decay reactions and to reduce the atmospheric neutrino background for nucleon decay searches. A delayed-coincidence detection of a positron and a neutron capture offers a powerful way to identify low-energy anti-neutrinos via the inverse beta decay reaction $\bar{\nu}_e + p \rightarrow e^+ + n$. The subsequent neutron capture in water yields a photon pair: $n + p \rightarrow d + \gamma$ (2.2 MeV).

The new technique has been verified by measurements which exhibit a clear neutron signal in atmospheric neutrino data. The neutrino energy spectrum has been extended to lower energies ($E_\nu > 14$ MeV), as depicted in Fig. 6.

In searches for supernova relic neutrinos or GUT monopoles in Super-Kamiokande, nuclear de-excitation γ -rays induced by neutral current interactions of atmospheric neutrinos with ^{16}O are one of the major background sources {UENO #253}. Such events are studied with the T2K experiment, which started in January 2010. Its beam energy is typical to atmospheric neutrinos. A low-energy (4 – 30 MeV) event search has been performed in the T2K data. This yields a better understanding

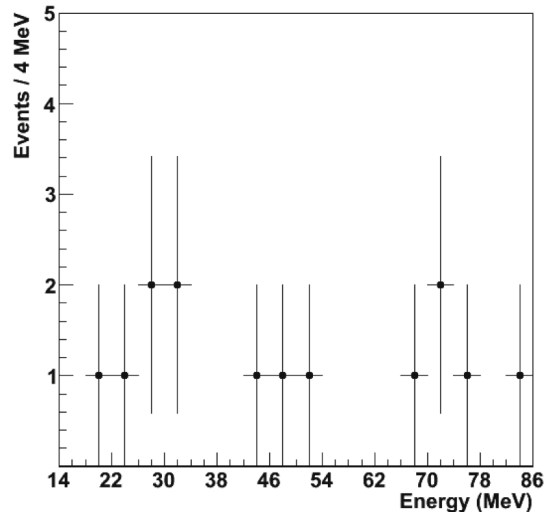


Figure 6: Neutrino energy spectrum ($E_\nu > 14$ MeV) reconstructed with neutron tagging in Super-Kamiokande {ZHANG #353}.

of the low-energy background.

The improved sensitivity is used to search for neutrinos from distant supernovae {SMY #855}. No evidence of a signal has been found. An upper limit (90% c.l.) on the neutrino flux has been established of about 2.7 neutrinos/cm²/s above 17.3 MeV neutrino energy.

3.4 ICARUS

The ICARUS detector, located at the Gran Sasso Underground Laboratory is composed of a big liquid argon time projection chamber (TPC), containing 600 t of liquid argon {COCCO #1340}. ICARUS is detecting neutrinos from the CNGS beam, produced at CERN and reaching Gran Sasso after a flight of about 730 km under the Earth surface. Data-taking has started in October 2010 and the first neutrinos from the CNGS beam have been measured at Gran Sasso. The time projection chamber exhibits excellent imaging capability together with good spatial and calorimetric resolutions. The main goal is to search for $\nu_\mu \rightarrow \nu_\tau$ oscillations in the neutrino beam from CERN. The expected sensitivity in the $\Delta m^2 - \sin^2(2\Theta)$ plot is expected to fully cover the LNSD-allowed region below $\Delta m^2 < 1 \text{ eV}^2/c^2$.

3.5 LVD

The Large Volume Detector (LVD), located at the Gran Sasso Underground Laboratory, is a 1 kt liquid scintillator neutrino observatory, mainly designed to study low-energy neutrinos from gravitational stellar collapses in the Galaxy {FULGIONE #513}. The experiment has been taking data since June 1992, with increasingly larger mass configurations. The telescope duty cycle, in the last ten years, has been greater than 99%. Recent results include the search for neutrino bursts, analyzing data from May 1st, 2009 to March 27th, 2011, for a total lifetime of 696.32 days. No evidence could be found for neutrino bursts from gravitational stellar collapses over the whole period under study. Considering the null results from previous measurements, it is concluded that no neutrino burst candidate has been found over 6314 days of lifetime, during which LVD has been able to monitor the whole Galaxy. A 90% c.l. upper limit on the rate of gravitational stellar collapses in the Galaxy ($D \leq 20$ kpc) has been established at 0.13 events/year.

4 HE 2.3 Neutrino telescopes and neutrino astronomy

Large-scale neutrino telescopes, such as IceCube or ANTARES, are Čerenkov detectors deployed deep in the Antarctic ice or in the ocean.

4.1 Atmospheric neutrino (and muon) flux

Most of the particles registered with water/ice Čerenkov telescopes are muons and neutrinos from air showers, induced by high-energy cosmic rays in the atmosphere. The basic idea is that downgoing muons are interpreted as muons from air showers above the detector, and muons moving upwards are interpreted as products of neutrinos generated in air showers on the other side of the Earth.

Relativistic muons passing through matter lose energy by various processes. The most common one is ionization of water molecules. Above 1 TeV, radiative processes start to dominate, leading to an almost linear dependence of the energy loss per unit length on the energy of the muon. Pair production, bremsstrahlung, and photo-nuclear interactions are the processes that are responsible for the increase of energy losses at higher energies.

The IceCube collaboration has measured the energy spectrum of downgoing (atmospheric) muons for energies from about 1 TeV up to around 500 TeV

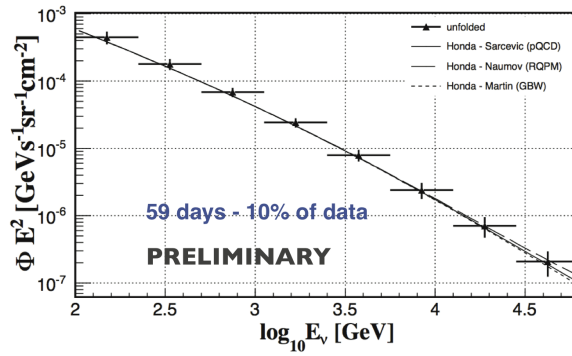


Figure 7: Atmospheric neutrino spectrum as measured by ANTARES {PALIOSELITIS #541}.

{BERGHAUS #85}. A method has been developed to identify TeV-scale catastrophic energy losses along muon tracks. It is applied to the separation of single high-energy muons from large-multiplicity bundles that dominate the event sample above the horizon at high energies. The information is used to derive the single-muon energy spectrum at all zenith angles. The observed muon flux is sensitive to the composition of cosmic rays. The measured energy spectrum of stochastic losses was compared to simulations based on various primary composition models [8]. The measurements are compatible with a cutoff of the proton flux at the knee in the energy spectrum of cosmic rays.

The ANTARES collaboration also investigates the sensitivity of the down-going muon flux to the composition of cosmic rays {HSU #679}. Several observational parameters are combined in a multiple-layered neural network to estimate the relative contribution of light and heavy cosmic rays.

The energy losses of muons are used by the ANTARES Collaboration to derive the corresponding muon energy {PALIOSELITIS #541}. An unfolding method is applied to derive the spectrum of atmospheric neutrinos from the measured muon flux. The result is depicted in Fig. 7.

Neutrinos in air showers originate from the decay of π and K mesons (the conventional flux) and from the decay of charmed mesons (the prompt flux). At TeV energies, where atmospheric neutrinos are an inevitable source of background events for astrophysical neutrino searches, the prompt flux becomes important and the flux predictions vary greatly. IceCube has measured the conventional atmospheric muon neutrino flux [9]. In addition, methods are developed to search for prompt neutrinos {MIDDELL #1097}. Data analysis with 40 strings of IceCube is under way.

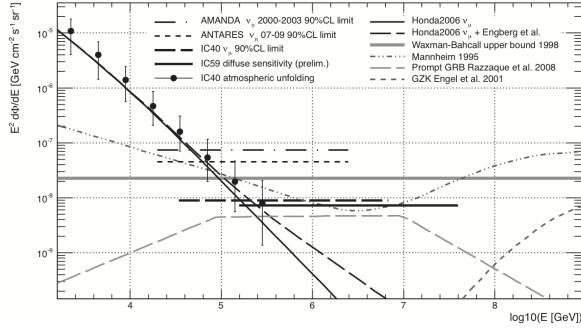


Figure 8: Limit on the diffuse neutrino flux derived by IceCube {SCHUKRAFT #736}.

4.2 Diffuse neutrino flux

The search for a cumulative flux of high-energy neutrinos from the sum of all cosmic sources in the Universe is one of the central goals of neutrino telescopes. The experimental signature of isotropically distributed astrophysical sources is an excess of high-energy neutrinos with a characteristic angular distribution over the background of less energetic neutrinos produced when cosmic rays interact with the Earth's atmosphere. Such searches are challenging because of systematic uncertainties in these fluxes and the detector response.

The measured flux of high-energy cosmic rays has been used to derive upper bounds on the expected diffuse neutrino flux [10, 11, 12]. In the TeV to PeV energy range, this flux is typically assumed to originate from particle interactions at or close to the cosmic-ray acceleration sites. Although only weakly constrained, the neutrino energy spectrum is typically modeled by a simple power law $\propto E^{-2}$. Therefore, limits on the diffuse neutrino flux are typically presented by multiplying the flux with E^2 .

The distribution of reconstructed neutrino energies in IceCube is analyzed using a likelihood approach that takes into account these uncertainties and simultaneously determines the contribution of an additional diffuse extraterrestrial neutrino component {SCHUKRAFT #736}. This analysis is applied to the data measured with the IceCube detector in its 40- and 59-string configurations, covering the period from April 2008 to May 2010. No evidence for an astrophysical neutrino flux was found in the 40-string analysis. The upper limit obtained for the period from April 2008 to May 2009 is $d\Phi/dE \leq 8.9 \cdot 10^{-9} \text{ GeV}^{-1} \text{ cm}^{-2} \text{ s}^{-1} \text{ sr}^{-1}$ at 90% c.l. in the energy region between 35 TeV and 7 PeV. For the 59-string data from May 2009 to May 2010, an improved analysis technique has been developed. The preliminary sensitivity is $d\Phi/dE \leq$

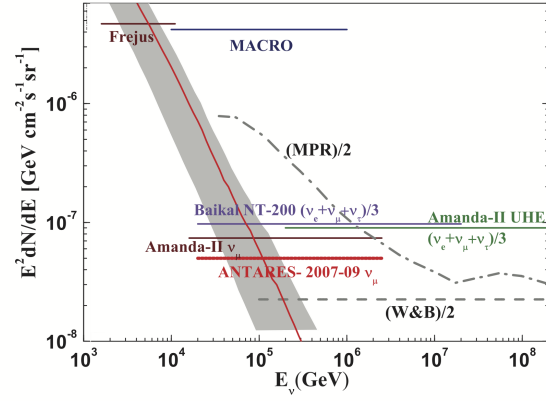


Figure 9: The upper limit for a E^{-2} diffuse high-energy ν_μ and $\bar{\nu}_\mu$ flux derived from data of the ANTARES neutrino telescope compared to previous measurements and phenomenological upper bound predictions {SCHÜSSLER #237}.

$7.2 \cdot 10^{-9} \text{ GeV}^{-1} \text{ cm}^{-2} \text{ s}^{-1} \text{ sr}^{-1}$. The flux limits are shown in Fig. 8.

Recent results on upper limits for the diffuse neutrino flux obtained by ANTARES {SCHÜSSLER #237} {HEIJBOER #858} are shown in Fig. 9. ANTARES obtained an upper limit of $E^2\Phi_{90\%} = 5.3 \cdot 10^{-8} \text{ GeV cm}^{-2} \text{ s}^{-1} \text{ sr}^{-1}$. The recent upper limits are in the range where neutrinos are expected according to the above mentioned calculations in the energy range $\approx 0.1 - 10 \text{ PeV}$.

The Surface Detector of the Pierre Auger Observatory can also be used to detect ultra-high-energy neutrinos in the sub-EeV energy range and above {GUARDINCERRI #682}. Neutrinos of all flavors can interact in the atmosphere and induce inclined showers close to the ground (down-going). The sensitivity of the Surface Detector to tau neutrinos is further enhanced through the "Earth-skimming" mechanism (up-going). Both types of neutrino interactions can be identified through the broad time structure of the signals induced in the Surface Detector stations. Two independent sets of identification criteria were designed to search for down and up-going neutrinos in the data collected from 1 January 2004 to 31 May 2010, with no candidates found. Assuming a differential flux $\Phi(E_\nu) = kE^{-2}$, a 90% c.l. upper limit on the single-flavor neutrino flux has been derived of $k < 2.8 \cdot 10^{-8} \text{ GeV cm}^{-2} \text{ s}^{-1} \text{ sr}^{-1}$ in the energy interval $\approx 10^{17} - 10^{19} \text{ eV}$ based on Earth-skimming neutrinos and $k < 1.7 \cdot 10^{-7} \text{ GeV cm}^{-2} \text{ s}^{-1} \text{ sr}^{-1}$ in the energy interval $\approx 10^{17} - 10^{20} \text{ eV}$ based on down-going neutrinos.

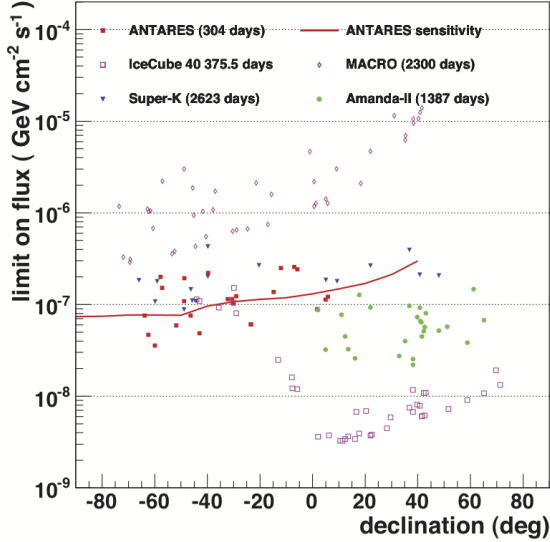


Figure 10: Limits set on the normalization of an E^{-2} spectrum of high-energy neutrinos from selected source candidates as obtained by ANTARES {BOGAZZI #295}.

4.3 Point sources

The observation of a deficit of cosmic rays from the direction of the Moon is an important experimental verification of the absolute pointing accuracy of a neutrino telescope and the angular resolution of the reconstruction methods. Both, ANTARES {RIVIERE #98} and IceCube {BOERSMA #1235} have reported an observation of the shadow of the Moon in the flux of down-going muons.

Several methods have been presented to search for (astrophysical) point sources in the measured arrival directions of neutrinos.

Clustering of neutrino arrival directions would provide hints for their astrophysical origin. The two-point autocorrelation method is sensitive to a large variety of cluster morphologies and provides complementary information to searches for the astrophysical sources of high-energy muon neutrinos. The autocorrelation function has been investigated as a function of the angular scale of data collected during 2007–08 with the ANTARES neutrino telescope {SCHÜSSLER #238}. The data, taken during the deployment phase of the detector, do not show evidence for deviations from the isotropic arrival direction distribution expected for the background of atmospheric neutrinos and contamination by misreconstructed atmospheric muons.

The first two years of ANTARES data (2007–08) have been used to search for point sources

{BOGAZZI #295} {GOMEZ-GONZALEZ #678}. No statistically significant excess of events has been found either in the search using a candidate list of 24 interesting (gamma-ray) sources, or in a full-sky search. The obtained flux limits are plotted as function of declination in Fig. 10. The most significant cluster, with a post-trial probability of 18%, corresponds to the location of HESS J1023-575.

The data from IceCube-40 and AMANDA, taken during 2008–09, are used to search for neutrino sources within the Galaxy {ODROWSKI #320}. The TeV gamma-ray spectra of some potential Galactic cosmic-ray accelerators show cut-offs in the energy spectrum at energies of a few TeV. In the case of transparent TeV gamma-ray sources, high-energy neutrinos will have similar spectra, and an improved effective area below a few TeV improves the sensitivity for these sources. Several tests, including a scan of the Galactic plane in the Northern Hemisphere and a dedicated analysis for the Cygnus region, have been performed. In the absence of a significant signal, upper limits have been obtained. The strongest preliminary flux limit can be set for Cas A at a flux of $5.9 \cdot 10^{-11} \text{ TeV}^{-1} \text{ cm}^{-2} \text{ s}^{-1}$.

With 55 events observed within the box defined around the most active part of the Cygnus region compared to a background expectation of 60 events, strong flux upper limits could be extracted for this region. Assuming an $E^{-2.6}$ spectrum, as obtained from the MILAGRO gamma-ray observations, a preliminary 90% flux upper limit of $3 \cdot 10^{-11} \text{ TeV}^{-1} \text{ cm}^{-2} \text{ s}^{-1}$ (without systematic uncertainties) is obtained, provided the astrophysical signal from the region has an exponential energy cutoff at or above 1 TeV.

The results provide the most restrictive upper limits for the Cygnus region obtained so far. Depending on the assumed energy cut-off, the upper limits obtained with this analysis are only a factor of two to three above the expected neutrino flux if all the TeV gamma-rays observed in the region were of hadronic origin. This implies that during the coming years, IceCube will be able to either detect neutrinos from the Cygnus region, or to constrain the nature of the high-energy gamma-ray emission in the region and, thus, the fraction of interacting cosmic rays produced in one of the most active parts of the Galaxy.

The Pierre Auger Observatory has also placed limits on the neutrino flux from point-like sources as a function of declination {GUARDINCERRI #682}. In particular, an upper limit has been set on neutrinos from the active galaxy Centaurus A. This Active Galactic Nucleus (AGN) is an interesting source, since there seems to be an enhancement

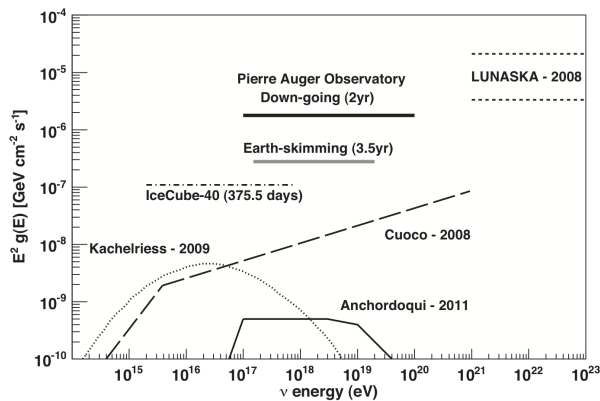


Figure 11: Single-flavor neutrino flux limits (90% c.l.) on Centaurus A as obtained by the Pierre Auger Observatory compared to model predictions {GUARDINCERRI #682}.

of charged cosmic rays from the direction of this source [13]. The obtained 90% c.l. upper neutrino flux limit is shown in Fig. 11. The present upper limits are still about 2 orders of magnitude above the expectations from theoretical models for this source.

4.4 Multi messenger searches

The correlation of information from different messenger particle types is of great astrophysical interest to identify the sources of high-energy particles. According to the standard theory of acceleration in astrophysical sources, charged (hadronic) particles are accelerated in the source and are expected to be accompanied by gamma-rays and neutrinos from pion decays formed in the interactions of hadrons with the surrounding medium at the sources. While gamma-rays have been linked to astrophysical sources by many experiments (H.E.S.S., MAGIC, VERITAS, Fermi), no point source of high-energy neutrinos has been found so far. Several investigations have been conducted, combining the search for high-energy neutrinos with photons, charged cosmic rays, and gravitational waves.

Neutrino multiplets observed with IceCube are used to send a trigger to the Robotic Optical Transient Search Experiment, ROTSE {FRANCKOWIAK #445}. The four ROTSE telescopes immediately observe the corresponding region in the sky in order to search for an optical counterpart to the neutrino events. Data from the first year of operation of the optical follow-up program have been searched for a signal from supernovae. No statistically significant excess in the rate of neutrino multiplets has been observed, and furthermore, no coincidence with an

optical counterpart was found during the first year of data-taking. This restricts current models, that predict a high-energy neutrino flux from soft jets in core-collapse supernovae.

ANTARES is used to initiate optical follow-up observations to search for transient sources, such as gamma ray bursters (GRBs) and core-collapse supernovae {AGERON #90}. A fast online muon track reconstruction is used to trigger a network of small automatic optical telescopes. Such alerts are generated one or two times per month for special events, such as two or more neutrinos coincident in time and direction or single neutrinos of very high energy. Since February 2009, ANTARES has sent 37 alert triggers to the TAROT and ROTSE telescope networks and 27 of them have resulted in followup observations. So far, no optical counterpart has been detected.

IceCube has also been used to trigger the SWIFT x-ray satellite {HOMEIER #535}. SWIFT then scans the sky in the direction of the neutrino for a transient x-ray counterpart, e.g. an x-ray gamma-ray burst afterglow. The program started in February 2011. Until May 2011, one trigger has been forwarded to SWIFT. The total latency between the neutrino events and the first observation by SWIFT was 90 minutes.

Finally, there are also plans to use IceCube as trigger for imaging atmospheric Čerenkov telescopes {FRANKE #334}. A test run has been conducted in early 2011. Interesting events have been identified, but triggers are (not yet) forwarded to a ground-based Čerenkov telescope.

In the reverse direction, data from the GRB coordinates network [14] were used to initiate a search for neutrinos with IceCube {REDL #764}. The analysis of data from the IceCube 59-string configuration is a dedicated search for neutrinos produced via $p - \gamma$ interactions in the prompt phase of the GRB fireball. Yielding no significant excess above the background, this constrains current models of GRBs.

ANTARES data are used to search for neutrinos from known astrophysical objects. Radio-loud active Galactic nuclei with their jets pointing almost directly towards the observer, the so-called blazars, are particularly attractive potential neutrino point sources {DORNIC #91}. The gamma-ray light curves of blazars measured by the Fermi LAT instrument reveal time variability information. An unbinned method based on the minimization of a likelihood ratio was applied to a subsample data collected in 2008 (61 days lifetime), by looking for neutrinos detected in the high state periods of the

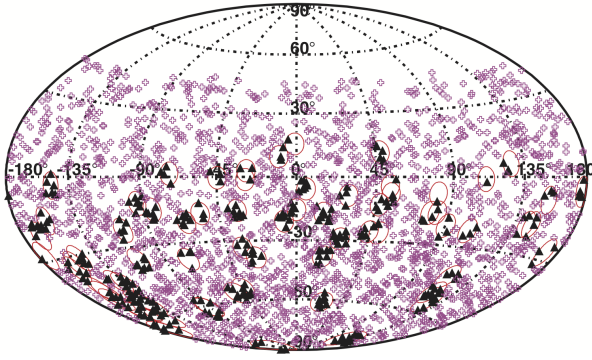


Figure 12: Skymap showing the arrival direction of neutrinos observed by ANTARES (crosses) and cosmic rays as measured by the Pierre Auger Observatory (triangles) {PETROVIC #291}.

AGN light curve. The search has been applied to ten very bright and variable Fermi LAT blazars. The most significant observation of a flare is 3C279, with a chance probability of about 10 % after trials, for which one neutrino event has been detected in time/space coincidence with the gamma-ray emission. Limits have been obtained on the neutrino fluence for the ten selected sources.

In 2007 ANTARES consisted of five detector lines. These data have been used to search for coincidences between the observed neutrinos and 37 GRBs {REED #1085}. No correlations have been observed.

A search for correlations between high-energy neutrinos and (charged) cosmic rays has been performed {PETROVIC #291}. A source-stacking analysis has been developed and applied to neutrino-candidate events detected during 2007 – 08 with the ANTARES neutrino telescope and 69 ultra-high-energy cosmic rays observed by the Pierre Auger Observatory. The corresponding arrival directions are depicted in a skymap in Fig.12. The observed number of correlated neutrino events is below expectations (negative correlation), with a significance of about 1.8σ . This result is compatible with a background fluctuation. The corresponding upper flux limit, assuming an equal flux from all ultra-high-energy cosmic-ray sources, is $5.43 \cdot 10^{-8} \text{ GeV cm}^{-2} \text{ s}^{-1}$.

Cataclysmic cosmic events can be plausible sources of both, gravitational waves and high-energy neutrinos. Both are alternative cosmic messengers that may traverse very dense media and travel unaffected over cosmological distances, carrying information from the innermost regions of the astrophysical engines. Such messengers could also reveal new, hidden sources that were not ob-

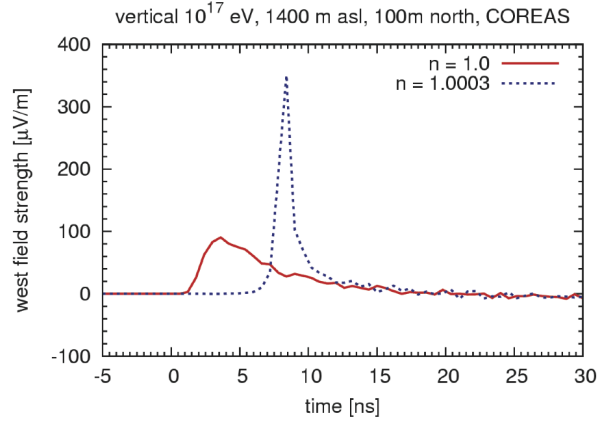


Figure 13: Radio emission from air showers. Expected field strength as function of time for media with two different refractory indices {HUEGE #653}.

served by conventional photon astronomy {VAN ELEWYCK #701}. A joint search was conducted with the ANTARES neutrino telescope and the LIGO/VIRGO gravitational wave detectors using concomitant data taken in 2007 during the VIRGO VSR1 and LIGO L5 science runs, while ANTARES was operating in a 5-line configuration. No coincident events have been found so far.

5 HE 2.4 Theory and calculations

5.1 The endpoint formalism

Huege *et al.* propose a formalism suitable for the calculation of electromagnetic radiation from any kind of particle acceleration, which lends itself very well to the implementation in Monte Carlo codes, and necessitates no simplifying approximations to the underlying processes {HUEGE #653}. In this "end-point formalism", presented in detail in Ref. [15], the trajectory of individual particles is described as a series of points at which particles are accelerated instantaneously, leading to discrete radiation contributions which can then be easily superimposed. The endpoint formalism can be applied in both, the frequency and time domains, and correctly reproduces several electromagnetic processes, like synchrotron radiation, Čerenkov radiation, and transition radiation. Furthermore, the authors demonstrate how the application of the end-point formalism provides insights to radio emission processes in astroparticle physics.

As an example for an application of the method,

predictions for the radio emission in air showers are shown in Fig. 13. It depicts the expected field strength at ground level as function of time for two assumptions for the refractive index of air. A more realistic index of $n > 1$ yields a sharper radio pulse.

5.2 Atmospheric neutrino spectrum

High-energy neutrinos, arising from decays of mesons produced through the collisions of cosmic-ray particles with air nuclei, form a background for the detection of astrophysical neutrinos {SINEGOVSKY #487}. An ambiguity in the high-energy behavior of pion and especially kaon production cross sections for nucleon-nucleus collisions may affect the calculated neutrino flux. The authors present results of the calculation of the energy spectrum and zenith-angle distribution of muon neutrinos and electron neutrinos of atmospheric origin in the energy range from 10 GeV to 10 PeV. The calculations were performed using several hadronic interaction models (QGSJET-II, SIBYLL 2.1, Kimel & Mokhov) and two parameterizations of the primary cosmic-ray spectrum, by Gaisser & Honda and by Zatsepin & Sokolskaya. The results demonstrate a weak dependence on the two models used for the primary cosmic-ray composition. The predicted fluxes are compared to measurements by the Frejus, AMANDA, and Ice-Cube experiments. This comparison indicates that QGSJET-II is the preferred model to describe the data. An analytic description of the calculated neutrino fluxes is given, for details see {SINEGOVSKY #487}.

5.3 Neutrino cross section

A new calculation has been presented of the cross sections for charged current and neutral current neutrino-nucleon and anti-neutrino-nucleon interactions in the neutrino energy range $10^4 < E_\nu < 10^{12}$ GeV [16] {CONNOLLY #1283}. The parton distribution functions have been used as calculated by A.D. Martin *et al.* known as "MSTW 2008". The latter incorporates improvements in the precision and kinematic range of recent measurements as well as improved theoretical developments that make the global analysis more reliable. The calculated neutrino-nucleon cross section is depicted in Fig. 14. Good agreement is found between the new calculations and previous results.

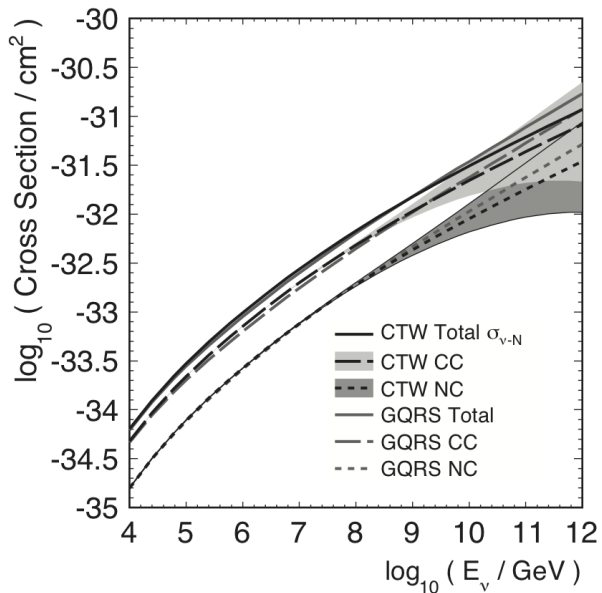


Figure 14: Calculated neutrino-nucleon cross section for charged-current and neutral-current reactions. For details, see [16] {CONNOLLY #1283}.

6 HE 2.5 Muon and neutrino tomography

6.1 Geophysical application

The capability of high-energy atmospheric muons to penetrate large depths of material makes them a unique probe for geophysical studies. Provided the topography is known, the measurement of the attenuation of the muon flux permits the cartography of density distributions, revealing spatial and possibly also temporal variations in extended geological structures. A collaboration between volcanologists, astroparticle- and particle physicists has been formed to study tomographic muon imaging of volcanos with high-resolution tracking detectors {FEHR #671}.

To achieve high resolution and low noise conditions, a muon telescope has been constructed, consisting of three planes of glass resistive plate chambers. A 1 m² chamber is read out by 9142 electronic channels.

First measurements have been conducted at the Puy de Dome, an inactive volcanic dome in south-central France. The shadow cast in the atmospheric muon flux has been observed. A reference region in the open sky is used to define an unabsorbed muon flux. This reference flux can be used to determine the absorption of muons in the volcano. The column density along trajectories crossing the detec-

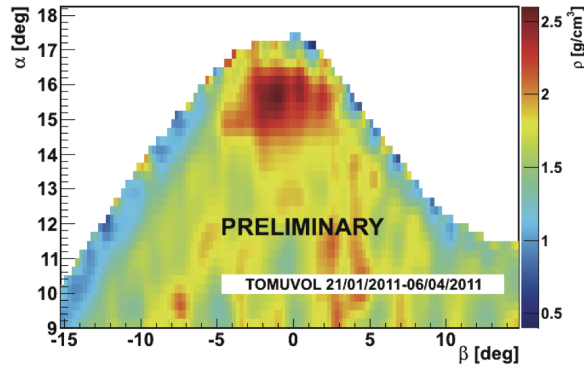


Figure 15: Measured average matter densities within the Puy de Dome along trajectories crossing the detection site 2 km off and 600 m below the summit. The measurement is based on 65.8 days of data-taking {FEHR #671}.

tion site can be extracted, see Fig. 15. The density map exhibits two features: a band of lower density at the flanks and a region with higher density just beneath the summit.

6.2 Archaeological application

The Pyramid of the Sun, at Teotihuacan, Mexico, is being searched for possible hidden chambers, by means of muon attenuation measurements inside the pyramid's volume {MENCHACA-ROCHA #1117}. A muon tracker is located in a tunnel, running below the base and ending close to the symmetry axis of the monument. The experimental setup, with an active area of 1 m × 1 m consists of six layers of 200-wire multiwire proportional chambers, interspaced with four layers of plastic scintillator planes, read out by wavelength shifter bars.

The muon transport through the pyramid is simulated using GEANT4. The pyramid shape is constructed from aerial photographs. The muon flux inside the pyramid has been measured for six months and compared to expectations from the simulations. The comparisons show qualitative and quantitative resemblances. Given the limited statistics accumulated so far, it is still too early to confirm or disprove the possibility of a human-size hidden empty cavity within the pyramid's volume.



Figure 16: Digital Optical Module (DOM) of the KM3NeT neutrino telescope. It consists of photo-multipliers with light concentrator rings, foam support, an aluminum cooling structure, and a cable feed-through {KOOIJMAN #800}.

7 HE 2.6 New experiments and instrumentation

The status of several endeavors to build new detectors for the measurement of high-energy neutrinos have been presented.

Dedicated high-energy neutrino telescopes based on optical Čerenkov techniques have been scanning the cosmos for about a decade. Consequently, neutrino flux limits have improved by several orders of magnitude in the TeV-PeV energy interval. At higher energies, detectors using radio Čerenkov techniques have produced aggressive limits on the neutrino flux.

7.1 KM3NeT

The KM3NeT project is aiming to construct a multi-km³ water Čerenkov neutrino telescope {KOOIJMAN #800}. Its envisaged location in the deep Mediterranean Sea optimizes the sensitivity for neutrino sources near the Galactic center. In 2010/11 a number of major decisions have been made on the technical implementation. A design has been adopted based on a digital optical module (DOM) configuration, housing many small photo-multipliers rather than earlier traditional designs, having a single large PMT. A DOM is depicted in

Fig.16. The readout electronics are incorporated into this digital optical module. The site-to-shore communication is provided by an electro-optical cable, allowing unique color point-to-point communication between each DOM and the shore station readout system. There are plans to install a DOM within ANTARES for an in-situ test under realistic environmental conditions {POPA #386}. Each mechanical supporting structure consists of twenty 6 m long bars with a DOM at each end. The bars have a vertical separation of 40 m, giving the full structure a height of around 900 m. The foreseen budget allows for the construction of about 300 of such structural units. Together they will create an instrumented volume of between 5 and 8 km³. The sensitivity to point sources near the Galactic center is expected to surpass that of earlier telescopes by two orders of magnitude. Construction is planned to start in 2014.

7.2 The Askaryan radio array - ARA

The Askaryan radio array (ARA) has the objective to detect ultra-high-energy neutrinos in a dense, radio-frequency transparent medium via the Askaryan effect {HOFFMAN #1316}. It is built on the expertise gained by RICE, ANITA, and IceCube's radio extension in the use of the Askaryan effect in cold Antarctic ice. The goal is to install an antenna array in bore holes extending 200 m below the surface of the ice near the geographic South Pole. The unprecedented scale of ARA, which will cover a fiducial area of 200 km², was chosen to ensure the detection of the flux of neutrinos expected from the observation of a GZK-like feature by HiRes and the Pierre Auger Observatory via cosmic-ray interactions with the cosmic microwave background.

Funding to develop the instrumentation and install the first prototypes has been granted, and the first components of ARA were installed during the austral summer of 2010–2011 {CONNOLLY #1237}. Within 3 years of commencing operation, the full ARA will exceed the sensitivity of any other instrument in the 0.1 – 10 EeV energy range by an order of magnitude. The primary goal of ARA is to establish the absolute cosmogenic neutrino flux through a modest number of events.

In January 2011, a first prototype testbed station for ARA was deployed 1.8 km east of the IceCube detector, at approximately 30 m depth {CONNOLLY #1237}. It included ten antennas deployed in the ice and six antennas deployed at the surface, covering frequencies from 30 to 850 MHz. The surface

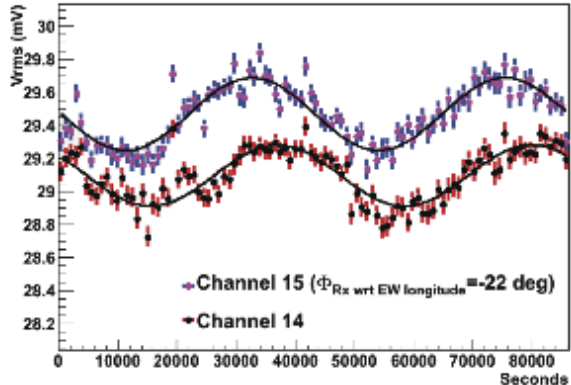


Figure 17: Radio background below 70 MHz as function of time of day as recorded by ARA {CONNOLLY #1237}.

antennas show an increase in thermal noise at frequencies below 150 MHz. This is consistent with Galactic radio noise, whose sky temperature follows the relation

$$T_{sky} = 800 \text{ K}(f/100 \text{ MHz}) - 2.5, \quad (1)$$

where f is the frequency. The radio background measured with two antennas is shown in Fig.17. One recognizes a sidereal modulation of the signal. Such a behavior is consistent with the observation of radio emission from the Galaxy, since the two surface antennas are low frequency dipoles with axes lying parallel to the surface and they sweep through the Galactic plane over a period of a day. The Galactic plane is at approximately 63° declination at the South Pole. The phase difference in the sine waves from the two antennas is due to an approximately 22° offset in orientation between them. The electronics of the currently deployed testbed detector are based on proven technology from the ANITA balloon experiment and further development of electronics is in progress {ALLISON #744}.

7.3 ARIANNA

A new concept for the detection of GZK neutrinos has been introduced — ARIANNA {BARWICK #976}. This next-generation astrophysical neutrino detector takes advantage of unique geophysical features of the Ross Ice Shelf in Antarctica. ARIANNA, based on the radio Čerenkov technique, is designed to improve the sensitivity to neutrinos with energies in excess of 10¹⁷ eV by at least a factor of 10 relative to current limits. The objective

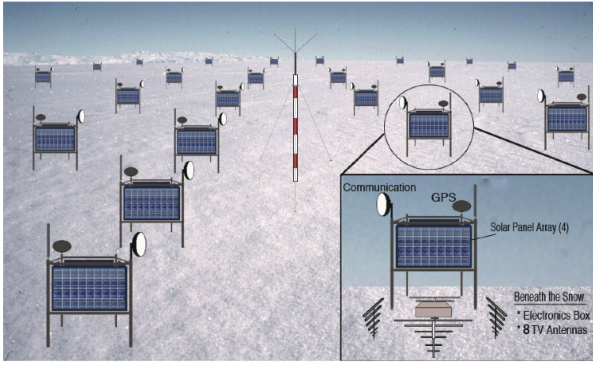


Figure 18: Schematic view of the ARIANNA experiment to measure neutrinos at the highest energies {BARWICK #976}.

of ARIANNA is a measurement of the GZK neutrino flux and the search for non-standard particle physics.

A schematic view of the planned set-up is shown in Fig. 18. The experiment will consist of autonomous radio detection stations on a hexagonal grid with a separation between stations of the order of 1 km. Each station will consist of in-ice radio antennas, a GPS receiver for timing, a solar panel array, and a communication unit. The first stage of ARIANNA was approved by the U.S. NSF in mid 2010.

First studies of the site properties have been conducted {HANSON #340}. Preliminary results in the frequency band 90 – 180 MHz confirm large attenuation lengths of (495 ± 15) m.

7.4 Acoustic neutrino detection

The AMADEUS system is an integral part of the ANTARES neutrino telescope in the Mediterranean Sea {LAHMANN #894}. The project aims for the investigation of techniques for acoustic neutrino detection in the deep sea. Installed at a depth of more than 2000 m, the acoustic sensors of AMADEUS are based on piezo-ceramic elements for the broad-band recording of signals with frequencies up to 125 kHz. AMADEUS was completed in May 2008 and is composed of six acoustic clusters, each one holding six acoustic sensors that are arranged at distances of roughly 1 m from each other. The clusters are installed with spacings ranging from 15 m to 340 m. Acoustic data are continuously acquired and processed at a computer cluster where online filter algorithms are applied to select a high-purity sample of neutrino-like signals. In order to assess the background of neutrino-like signals in the deep sea, the

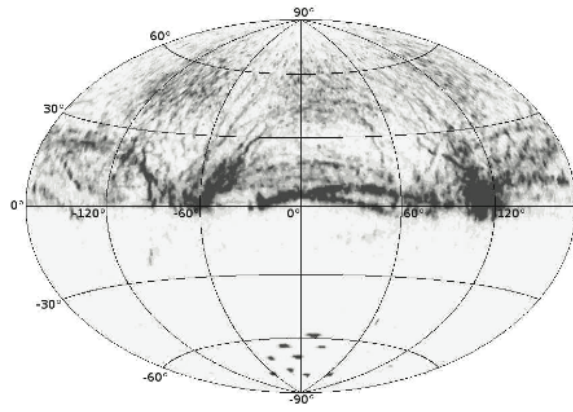


Figure 19: Map of directions of sources reconstructed with an acoustic detector (AMADEUS) in the ANTARES neutrino telescope {LAHMANN #894}.

characteristics of ambient noise and transient signals have been investigated.

A result of the measurements is depicted in Fig. 19. It shows a map of directions of reconstructed acoustic sources. Zero degrees in azimuth corresponds to the north direction and the polar angle of zero corresponds to the horizon of an observer on the acoustic storey. At the bottom, the signals of the emitters of the ANTARES positioning system are visible. The measurements of the ambient noise show that the noise level is very stable and at the expected level, allowing for measurements of neutrino energies down to ≈ 1 EeV.

7.5 Particle interactions on the Moon

High(est)-energy cosmic rays and neutrinos impinging on the Moon are expected to emit radio emission in the MHz regime. Such radiation is searched for with the LOFAR radio telescope {SCHOLTEN #86} {TER VEEN #1042}. At energies exceeding 10^{21} eV upper limits on the neutrino flux of the order of $E^2 dN/dE \approx 10^{-10} \text{ GeV cm}^{-2} \text{ sr}^{-1} \text{ s}^{-1}$ are expected for one week observation time.

8 HE 3.1 Hadronic interactions

The properties of cosmic rays at high energies are investigated through the measurement of extensive air showers, induced by high-energy particles in the atmosphere. The understanding of high-energy

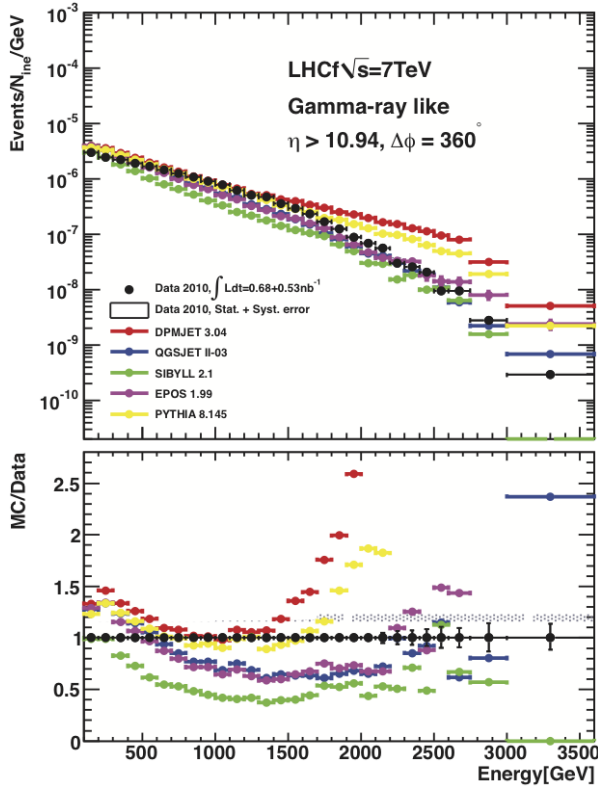


Figure 20: Single-photon energy spectrum in proton-proton interactions as measured by LHCf. The top panels shows the measured values together with predictions from hadronic interaction models. In the lower panel the ratio of predictions to measured values are displayed {MITSUKA #1000}.

hadronic interactions is crucial for a correct interpretation of the air shower data.

8.1 LHCf

First results from the Large Hadron Collider (LHC) open insight into a new energy regime, never covered before at a man-made accelerator. The energy range of the LHC is indicated on the upper scale in Fig. 22. Of particular interest for cosmic-ray physics is the LHCf experiment. It has two independent detectors, installed 140 m from the interaction point of the ATLAS experiment [17]. The principle idea is to measure charged particles as close as possible to the beam, investigating the forward direction with small momentum transfer, i.e. large pseudo rapidities $|\eta| > 4$.² The baseline set-up and upgrades

²The pseudo rapidity η describes the angle of a particle relative to the beam axis. Is is defined as $\eta = -\ln [\tan (\theta/2)]$, where θ is the angle between the particle momentum \vec{p} and the beam axis, or, using the longitudinal component p_L of the particle momentum $\eta = 1/2 \ln [(|\vec{p}| + p_L)/(|\vec{p}| - p_L)]$.

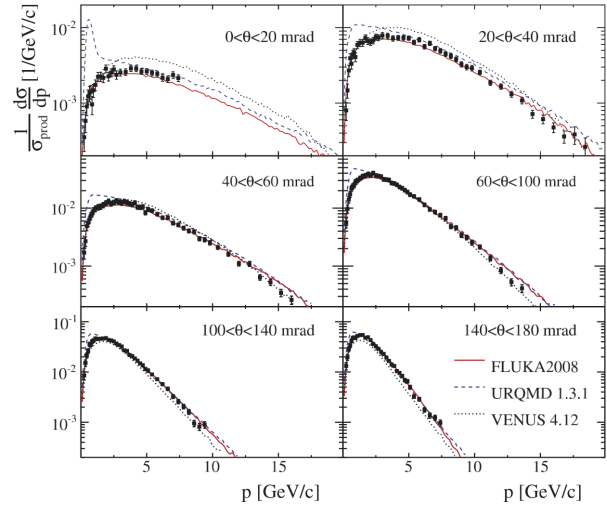


Figure 21: Momentum spectra of π^- in p+C interactions at 31 GeV/c measured by NA61 compared to predictions with FLUKA2008, URQMD1.3.1, and VENUS4.12 {UNGER #1094}.

of the experiment have been presented {SUZUKI #264} {NODA #421} {KAWADE #959}. The performance of LHCf was studied with SPS beams in 2007 {MASE #378}. A critical parameter for the analysis is the total luminosity, it can be determined with an accuracy on the 4 – 5% level {TAKI #374}.

The first phase of data-taking of LHCf has been finished in 2010 with proton-proton collisions at center-of-mass energies of $\sqrt{s} = 0.9$ and 7 TeV {SAKO #964}. As an example for recent results, the single-photon energy spectrum in forward direction ($\eta > 10.94$) is presented in Fig. 20 {MITSUKA #1000}. The results obtained with the two detectors on either side of the interaction point are consistent with each other and a combination of the results of both detectors is shown in the figure. In the top panel the measured values are compared to predictions of various hadronic interactions models used in the simulation of extensive air showers for cosmic-ray physics. The ratio of model predictions to data is displayed in the lower panel. It can be realized that none of the models used describes the measurements perfect. Such distributions are valuable to tune hadronic interaction models. Data from the LHCf experiment are expected to play a crucial role in the further development of hadronic interaction models in the near future.

8.2 NA61/SHINE

At lower energies (up to 350 GeV) the NA61/SHINE fixed-target experiment is studying

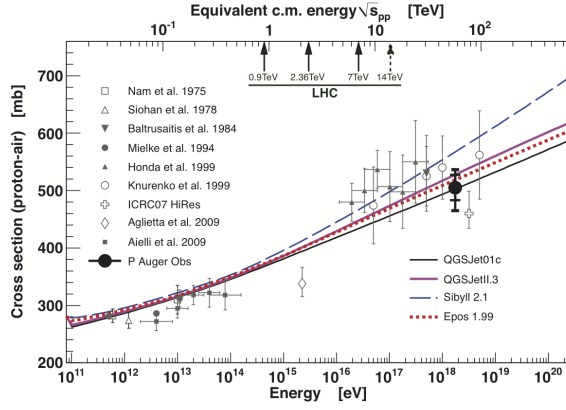


Figure 22: Proton-air cross section derived from air shower measurements with the Pierre Auger Observatory together with results from other experiments and predictions of hadronic interaction models {ULRICH #946}.

hadron production in hadron-nucleus and nucleus-nucleus collisions at the CERN SPS {UNGER #1094}. The physics program is optimized for cosmic-ray physics, e.g. investigating collisions of protons and pions with a carbon target. As an example for recent results, the momentum spectra of π^- in proton-carbon interactions at a momentum of 31 GeV/c are shown in Fig. 21. The different panels depict results for different angles between the secondary pions and the beam axis. The measured values are compared to predictions of hadronic interaction models used for air-shower simulations. Such comparisons are valuable for a further development of hadronic interaction models.

8.3 Proton-air and proton-proton cross sections

Air showers measured with the Pierre Auger Observatory have been used to derive the proton-air interaction cross section at a center-of-mass energy of 57 TeV {ULRICH #946}. Air showers observed with the fluorescence detector and at least one station of the Surface Detector array are analyzed in the energy range from 10^{18} to $10^{18.5}$ eV. A fit to the tail of the observed distribution of shower maxima yields a value of $\Lambda = (55.8 \pm 2.3_{stat} \pm 0.6_{syst})$ g/cm² for the attenuation length. Emphasis is given to systematic uncertainties in the cross section estimate arising from the limited knowledge of the primary mass composition, the need to use shower simulations, and the selection of showers. For the calculation of the proton-air cross section one of the main uncer-

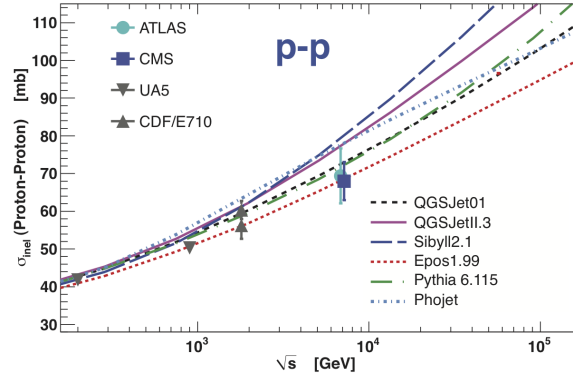


Figure 23: Proton-proton cross section as recently measured at the LHC ($\sqrt{s} = 7$ TeV) and earlier results from UA5 and CDF compared to predictions of hadronic interaction models, after {ULRICH #946}.

tainties is the unknown mass composition of cosmic rays. In particular, a (unknown) contribution of helium nuclei is expected to bias the obtained values. This influence has been systematically studied. For the proton-air cross section at (57 ± 6) TeV a value of

$$\sigma_{p-air} = \left(505 \pm 22_{stat} \left(\begin{smallmatrix} +20 \\ -15 \end{smallmatrix} \right)_{syst} \right) \text{ mb}$$

has been derived. The helium-induced systematics is -12 , -30 , and -80 mb for a helium contribution of 10%, 25%, and 50%, respectively. The bias due to photons in cosmic rays is < 10 mb. The value obtained is shown in Fig. 22 together with cross sections obtained in previous experiments.

The Auger Collaboration is about to derive the proton-proton cross section from the measured proton-air cross section at $\sqrt{s} = 57$ TeV. Recent measurements of the proton-proton cross section from the LHC experiments ATLAS and CMS at a center-of-mass energy of $\sqrt{s} = 7$ TeV are shown in Fig. 23.

In Figs. 22 and 23 predictions from hadronic interaction models, used for air-shower simulations are shown in addition to the experimental values. It should be noted, that the recent Auger results and the recent LHC measurements are at the lower boundary of the range predicted by the various interaction models.

8.4 Air shower data and models

The influence of recent LHC results on the interpretation of air-shower data has been investigated {PIEROG #1169}. Measurements by ALICE, ATLAS, and CMS indicate lower values for the

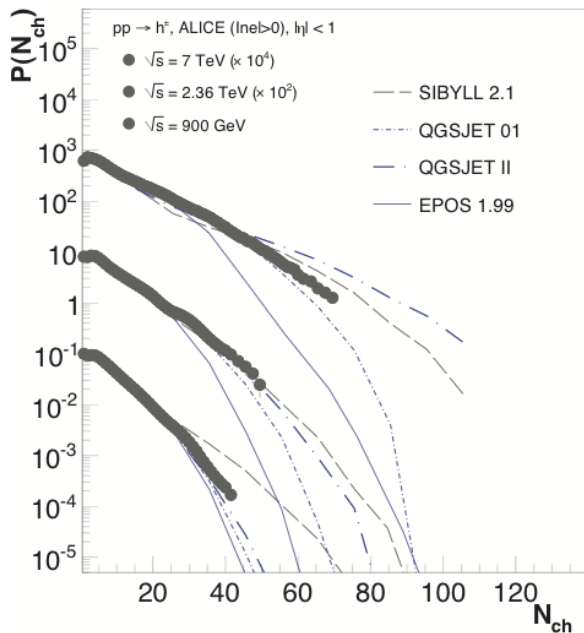


Figure 24: Multiplicity distributions of charged hadrons as measured by ALICE in proton-proton collisions at energies of $\sqrt{s} = 0.9, 2.26$, and 7 TeV compared to predictions of hadronic interaction models {PIEROG #1169}.

proton-proton cross section as predicted by current hadronic interaction models. If the models are adjusted to the new measurements one expects a shift of the depth of the shower maximum in air shower simulations. This implies that measurements of the shower maximum of air showers will yield a heavier mass composition of cosmic rays at high(est) energies.

Detailed investigations of pseudo rapidity and multiplicity distributions of charged secondary particles in proton-proton collisions indicate that the LHC data are bracketed by predictions of the hadronic interaction models QGSJET-II and EPOS 1.99. As an example, the multiplicity distribution of charged hadrons in proton-proton interactions as measured by ALICE is shown in Fig. 24. Results for different energies are compared to predictions of hadronic interaction models. Also distributions measured in forward direction by LHCf are under investigation. Small deviations are visible with respect to predictions of hadronic interaction models. However, the influence on the interpretation of air shower data is expected to be small as compared to the effect of the lower cross sections.

Studies of hadronic interactions are also under way at the ARGO-YBJ experiment {DE MITRI #754}.

The author would like to end this section with two remarks:

In the past, various ideas have been discussed as possible origin of the knee in the energy spectrum of cosmic rays, among them were ideas about new types of (hadronic) interactions in the atmosphere, see e.g. [18]. The recent LHC results exhibit a fair agreement with predictions of hadronic interaction models using standard physics. Hence, it can be concluded that the knee in the energy spectrum is not caused by new physics in the atmosphere, it is rather of astrophysical origin.

The recent results from the LHC (and the Pierre Auger Observatory) indicate lower values for the proton-air and proton-proton cross sections. A lower cross section has already been predicted in 2003 [19]. In this work the mean logarithmic mass derived from air shower observations has been systematically investigated. In particular, a discrepancy has been found between experiments observing the depth of the shower maximum and experiments registering the number of secondary particles at ground. It has been shown that a smaller proton-proton and consequently also proton-air cross section reduces the discrepancy in the derived mean logarithmic mass from the different classes of observables. The recent results confirm this earlier findings and this example illustrates how the new LHC measurements directly influence the interpretation of air shower data.

9 HE 3.3 Exotic particle searches

9.1 Magnetic monopoles

Magnetic monopoles are predicted by grand unified theories (GUT) {POSSELT #734}. The magnetic charge of a monopole is given by $g = Ne/2\alpha \approx 68.5 e$, where α is the fine structure constant, and e the elementary (electric) charge [20]. The mass of monopoles is expected to range from 10^8 to 10^{17} GeV for various GUT models. Because of these large masses magnetic monopoles are generally assumed to be relics of the early Universe. Analogous to electric charges, which are accelerated along electric field lines, magnetic monopoles are accelerated along magnetic field lines. During the lifetime of the Universe, relic monopoles should have encountered enough accelerators to reach kinetic energies of $\approx 10^{14}$ GeV. Thus, monopoles with masses less than $\approx 10^{14}$ GeV should be relativistic.

A water/ice Čerenkov detector is able to detect

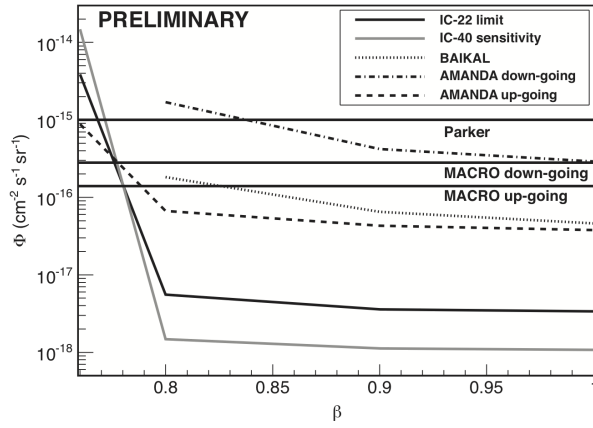


Figure 25: Monopole flux limits set by the 22-string IceCube detector, shown together with previous results {POSSELT #734}. Also shown is the expected 40-string sensitivity.

magnetic monopoles traveling through the detector at velocities greater than the Čerenkov threshold ($\beta > 0.76$). The radiation emitted by the monopole is proportional to $(gn)^2$, where n is the index of refraction of the ambient medium. Thus, in water/ice ($n \approx 1.3$) a monopole will emit almost 8000 times more light than a single muon of the same velocity.

Data taken with the 22-string IceCube detector were used to derive new upper limits on the monopole flux. The limits on the flux of magnetic monopoles with speeds $\beta > 0.8$ are shown in Fig. 25. They are presently the most stringent experimental limits to date. IceCube-40 is expected to reach a sensitivity of $10^{-18} \text{ cm}^{-2} \text{ s}^{-1} \text{ sr}^{-1}$.

A similar search has been performed with ANTARES {PICOT-CLEMENTE #695}. An upper limit has been derived, with values slightly above $10^{-17} \text{ cm}^{-2} \text{ s}^{-1} \text{ sr}^{-1}$ and, thus, slightly above the limits set by IceCube.

The imaging atmospheric Čerenkov telescope H.E.S.S. has also been used to search for monopoles. However, at present, these searches yield less stringent upper limits as compared to the neutrino telescopes {SPENGLER #864}.

9.2 Antinuclei

The asymmetry of particles and antiparticles in the Universe is one of the fundamental questions in cosmology {SASAKI #1230}. While antiprotons have been found in cosmic rays, so far no antiparticles with $|Z| \geq 2$ have been detected. Many cosmologists consider that this asymmetry was caused by the symmetry breaking between particles and antiparticles just after the Big Bang, with cosmo-

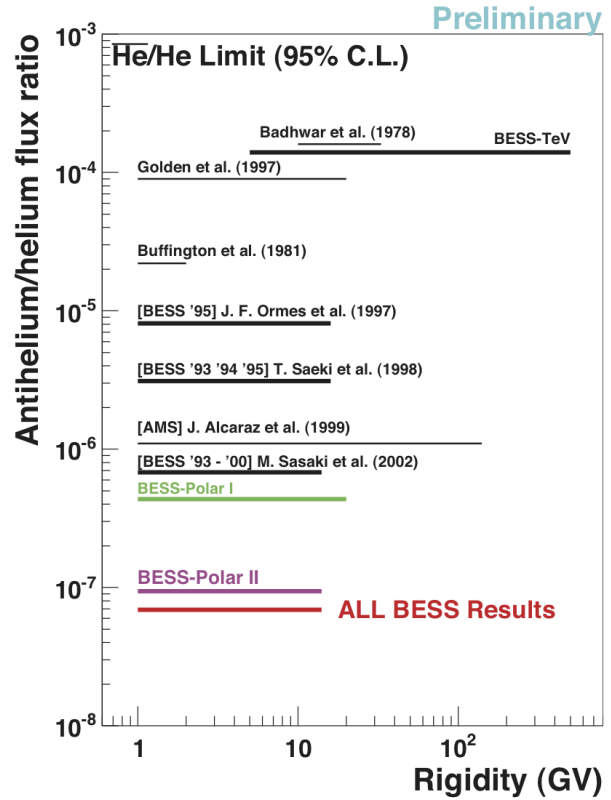


Figure 26: Upper limits on the ratio of antihelium to helium nuclei in cosmic rays as reported by the BESS experiment {SASAKI #1230}.

logical antiparticles vanishing at an early stage of the Universe. However, the existence of $|Z| \geq 2$ antiparticles is not excluded by theory. There might be remnant antiparticle domains from the Big Bang.

Therefore, the BESS Collaboration has conducted an extensive search for antinuclei in cosmic rays over the last 20 years {SASAKI #1230} {YOSHIMURA #1259}. The heart of BESS is a magnetic spectrometer to identify the sign of the throughgoing particles, and, thus, identify antiparticles. The set-up is complemented by time-of-flight counters and a silica aerogel Čerenkov counter. Various experimental configurations have been developed and flown on stratospheric balloons in the last two decades. Results from the latest version of the instrument, BESS-Polar II, have been reported.

The upper limits on the antihelium-to-helium ratio are depicted in Fig. 26. The sensitivity has improved over the last 20 years by a factor of 1000 – a quite impressive number. The recent results indicate that there is less than 1 antihelium nucleus per 10^7 helium nuclei in the Universe.

Searches for antideuterons are under way

{YOSHIMURA #1259}. No antideuteron has been found so far in cosmic rays. Upper limits are expected to be published soon.

9.3 Simultaneous air showers

The coincident detection of air showers from the same direction at the same time would be an experimental hint towards interesting physical processes. Among them are speculations about strangelets from cosmological origin or the break-up of cosmic-ray nuclei in the heliosphere.

A search for simultaneous showers was conducted at CERN for strangelets whose breakup in space may result in the arrival of a large number of time and angle-coincident air showers spread over a large area {TONWAR #1295}. Two shower detector arrays were used, located on the surface at points P2 and P4 at the LHC, which are separated horizontally by about 8 km. The arrival time of showers was recorded at each array with 100 ns accuracy, and the spatial arrival angle of showers was determined to an accuracy of about 3° . More than 10^7 showers were collected between 2004 and 2006.

No pairs of showers were detected arriving within $30 \mu\text{s}$ in time and within 5° in spatial angle at the two stations. This yields a 90% c.l. upper limit of $5.1 \cdot 10^{-20} \text{ cm}^{-2} \text{ sr}^{-1} \text{ s}^{-1}$ on the flux of strangelets.

A search was made for the interaction between cosmic rays and ions in the heliosphere using data collected by the HiRes-1 detector of the High Resolution Fly's Eye {RODRIGUEZ #1304}. Such an interaction could produce a jet containing neutral pions which can lead to an observation of an unique signature of parallel, simultaneous photon showers. The data were searched in a time window of $100 \mu\text{s}$. No coincident showers have been found.

10 HE 3.4 Direct and indirect dark matter searches

According the current standard model of cosmology, almost 25% of the energy budget of the Universe is an unknown, invisible mass component, the dark matter. Despite many efforts over the last years, dark matter is still one of the greatest mysteries of modern physics. The dark-matter particle could be a weakly interacting massive particle (WIMP). It is assumed that WIMPs were thermally produced in the early Universe, that they are stable, and of a non-baryonic nature [21]. Through self-annihilation, WIMPs should produce Standard Model particles, and some of the byproducts, like

photons, hadrons and leptons, might be observable at Earth. Supersymmetry (SUSY) provides a natural candidate for the dark-matter WIMP – the lightest SUSY particle neutralino.

Given the natural mass range for the SUSY WIMPs (between a few GeV and a few TeV) [22], it may be possible to find, via very energetic photons, some signatures for dark-matter annihilation in the energy range of imaging atmospheric Čerenkov telescopes {ALEKSIC #331}. The typical annihilation gamma-ray spectrum is predicted to be continuous and featureless, due to the gammas mainly being produced from pion decays and final-state radiation of charged particles. Nevertheless, some distinctive spectral features could be present, like the line emission (from WIMP annihilation into a pair of gammas or a gamma and a Z -boson), a cut-off or spectral hardening due to internal bremsstrahlung, with all of these dependent on the mass of the dark-matter particle.

The basic search strategy for indirect dark-matter searches is to look for high-energy gamma rays and neutrinos from the annihilation of dark-matter particles. Given that the annihilation rate is proportional to the dark-matter density squared, the best places to look for the WIMPs are astronomical regions with a large concentration of dark matter. Several recent activities have been discussed, such as looking for annihilation products in galaxy clusters, dwarf spheroidal galaxies, globular clusters, the Milky Way halo, or the Sun.

10.1 Galaxy clusters

Clusters of galaxies, such as the Virgo Cluster, host enormous quantities of dark matter, making them prime targets for efforts in indirect dark matter search. A multi-wavelength spectral energy distribution for the central radio galaxy in the Virgo Cluster, M87, has been constructed, using a state-of-the-art numerical synchrotron self Compton approach. Fitting recent Chandra, FERMI-LAT, and Čerenkov telescope observations, yields a best fit value for the neutralino mass of $m_\chi = 3.4 \text{ TeV}$ {SAXENA #204}.

10.2 Dwarf spheroidal galaxies

Dwarf spheroidals, the satellite galaxies of the Milky Way, have been identified as one of the most suitable candidates for dark-matter searches: the ratio between the mass inferred from gravitational effects and the mass inferred from luminosity (M/L) can reach values from 100 up to few

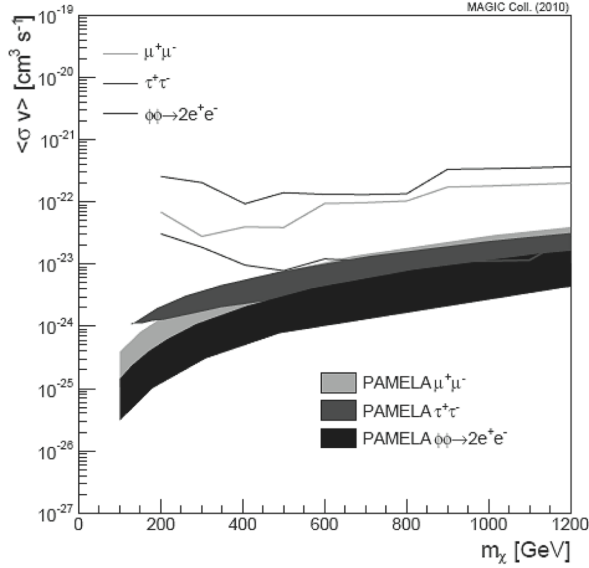


Figure 27: Upper limits on particular annihilation channels as obtained by MAGIC and corresponding regions that provide a good fit to PAMELA data {ALEKSIC #331}.

$1000 M_\odot/L_\odot$ for these objects. They are relatively close to the observer and they are expected to be free of astrophysical objects whose gamma-ray emission might hide the dark-matter signal {ALEKSIC #331}.

Until several years ago, only nine dwarf spheroidal galaxies were discovered orbiting the Milky Way. These, so-called classical dwarfs were joined by 11 new, ultra-faint objects thanks to the discoveries of the Sloan Digital Sky Survey (SDSS), starting in 2005. Among these objects several have been identified as excellent candidates for indirect dark-matter searches {ALEKSIC #331}.

Segue 1 is a ultra-faint object discovered in 2007 by the SDSS and located 23 kpc from the Sun. It is the most dark-matter dominated object known so far, with $M/L \approx 1320 - 3400 M_\odot/L_\odot$.

Segue 1 has been observed with the MAGIC Čerenkov telescope for 29.4 hours {ALEKSIC #331}. No significant gamma-ray signal was found above the background. The data have been used to probe dark-matter models that try to explain the PAMELA data, see Fig. 27. Current results are probing the PAMELA-preferred region for the case of dark-matter annihilation into $\tau^+ + \tau^-$.

Segue 1 has also been observed by VERITAS for almost 48 hours {VIVIER #919}. For the W^+W^- annihilation channel, a 95% c.l. upper limit on the velocity-weighted annihilation cross section $\langle\sigma v\rangle$ has been obtained at the level of $8 \cdot 10^{-24} \text{ cm}^3 \text{s}^{-1}$

around 1 TeV.

13 dwarf spheroidal galaxies (also among them Segue 1) have been observed by IceCube-59 to search for dark matter {LÜNEMANN #1024}. Sensitivities to the velocity-weighted dark matter self-annihilation cross section are better than $10^{-20} \text{ cm}^3 \text{s}^{-1}$, for WIMP masses in a range from 300 GeV to several TeV. These searches are complementary to gamma-ray observations in most channels and have the advantage that IceCube data of these sources are collected continuously and extend to higher WIMP masses.

The Sculptor and Carina dwarf spheroidal galaxies were observed with H.E.S.S. for 11.8 and 14.8 hours, respectively {VIANA #1036}. No gamma-ray signal was detected at the nominal positions of these galaxies above 220 GeV and 320 GeV, respectively. Constraints on the dark matter velocity-weighted annihilation cross section for both, the Sculptor and Carina dwarf galaxies range from $\langle\sigma v\rangle \approx 10^{-21}$ down to $10^{-22} \text{ cm}^3 \text{s}^{-1}$, depending on the dark-matter halo model.

10.3 Globular clusters

Several Galactic globular clusters have been observed with imaging atmospheric Čerenkov telescopes. Globular clusters are dense stellar systems with an age of about 10 Gyr, found in halos of galaxies, with typical masses between 10^4 and a few $10^6 M_\odot$. They are potential targets for indirect dark-matter searches.

The globular clusters NGC 6388 and M15 have been observed with H.E.S.S. for a lifetime of 27.2 and 15.2 hr, respectively {MOULIN #1121}. No gamma-ray signal is found at the nominal target positions. 95% c.l. exclusion limits on the dark matter velocity-weighted annihilation cross section $\langle\sigma v\rangle$ are derived for these dark matter halos. In the TeV range, these limits reach the $10^{-25} \text{ cm}^3 \text{s}^{-1}$ level and a few $10^{-24} \text{ cm}^3 \text{s}^{-1}$ for NGC 6388 and M15, respectively.

The Fornax galaxy cluster has been observed with H.E.S.S. for a total of 11 hours of lifetime. For a dark matter particle mass of 1 TeV, the exclusion limits reach values of $\langle\sigma v\rangle < 10^{-21} \text{ cm}^3 \text{s}^{-1}$, depending on the dark-matter model and halo properties {VIANA #1038}.

10.4 Milky Way halo

The central region of the dark-matter halo in the Milky Way is also a promising target for a search for a particle dark matter self-annihilation signal. With the IceCube neutrino telescope a search for WIMP

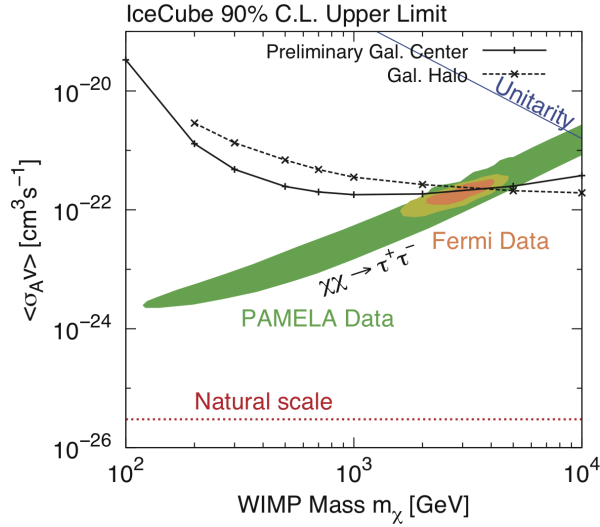


Figure 28: Limit on the velocity-weighted WIMP cross section $\langle\sigma v\rangle$ at 90% c.l. as function of the WIMP mass as obtained from observations of the Galactic Center with IceCube {ROTT #1187}. The preferred range obtained from gamma-ray observations with PAMELA and Fermi is indicated as well.

dark matter accumulated in the Galactic halo and the Galactic center has been conducted {ROTT #1187}. Limits on the dark matter velocity-weighted annihilation cross section $\langle\sigma v\rangle$ at a level of 10^{-22} to 10^{-23} $\text{cm}^3 \text{s}^{-1}$ have been achieved. The values obtained are shown in Fig. 28 as function of WIMP mass together with recent results from the PAMELA and Fermi gamma-ray space missions. The various experimental values nicely overlap for WIMP masses in the region 2 – 3 TeV.

Corresponding searches with the H.E.S.S. imaging atmospheric Čerenkov telescope are under way {SPENGLER #862}.

10.5 Sun

Another possibility to look for dark-matter signatures is the Sun, where dark matter could be gravitationally trapped. Dark matter could be indirectly detected through the observation of neutrinos produced as part of the self-annihilation process.

The IceCube neutrino telescope with the DeepCore sub-array is used to search for dark matter {DANNINGER #292}. This will lead to stringent constraints on WIMP-proton cross sections. The expected sensitivity of IceCube is illustrated in Fig. 29. For neutralino masses in the 100 GeV range, limits on the proton-neutralino cross section as low as 10^{-41} cm^2 are expected. Recent limits obtained with AMANDA and IceCube 40 are dis-

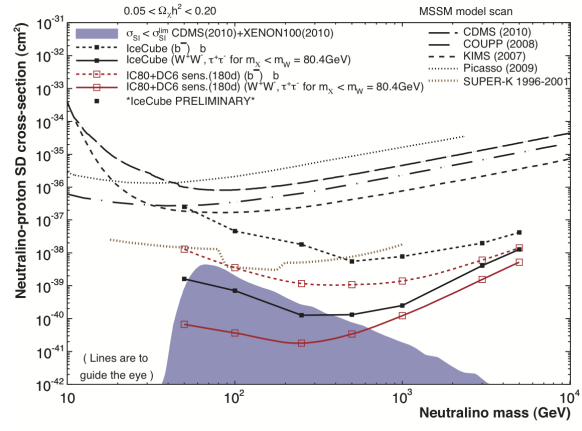


Figure 29: Sensitivity on the spin-dependent neutralino-proton cross section at 90% c.l. as function of the neutralino mass as obtained by IceCube {DANNINGER #292}.

cussed in {ENGDEGARD #327}.

ANTARES reports limits for the spin-dependent neutralino cross section, with sensitivities similar to the preliminary IceCube results {LAMBARD #202}.

11 Acknowledgments

The author would like to thank the organizers of the conference for their great hospitality in Beijing.

I'm grateful to John Kelley for critically reading the manuscript.

References

- [1] R. Abbasi, et al., arXiv 1105.2326 (2011).
- [2] R. Bernabei, et al., arXiv 1007.0595 (2010).
- [3] K. Blum, arXiv1110.0857 (2011).
- [4] U. Dore, D. Orestano, Rept. Prog. Phys. 71 (2008) 106201.
- [5] P. Adamson, et al., Phys. Rev. Lett. 106 (2011) 181801.
- [6] Y. Fukuda, et al., Phys. Rev. Lett. 81 (1998) 1562.
- [7] S. Fukuda, et al., Phys. Rev. Lett. 86 (2001) 5656.
- [8] J. Hörandel, Astropart. Phys. 19 (2003) 193.
- [9] R. Abbasi, et al., Phys. Rev. D83 (2011) 012001.

- [10] E. Waxman, J. N. Bahcall, Phys. Rev. D59 (1999) 023002.
- [11] J. N. Bahcall, E. Waxman, Phys. Rev. D64 (2001) 023002.
- [12] K. Mannheim, R. J. Protheroe, J. P. Rachen, Phys. Rev. D63 (2001) 023003.
- [13] P. Abreu, et al., Astropart. Phys. 34 (2010) 314.
- [14] GRB Coordinates Network, <http://gcn.gsfc.nasa.gov>.
- [15] C. W. James, H. Falcke, T. Huege, M. Ludwig, arXiv:1007.4146 (2010).
- [16] A. Connolly, R. S. Thorne, D. Waters, Phys.Rev. D83 (2011) 113009.
- [17] LHCf Collaboration, J. Instr. 3 (2008) S08006.
- [18] J. Hörandel, Astropart. Phys. 21 (2004) 241.
- [19] J. Hörandel, J. Phys. G: Nucl. Part. Phys. 29 (2003) 2439.
- [20] P. Dirac, Proc. Roy. Soc. A 133 (1931) 60.
- [21] G. Bertone, D. Hooper, J. Silk, Phys. Rept. 405 (2005) 279.
- [22] G. Bertone, (ed.), Cambridge, UK: Univ. Pr. (2010) 738 p.